NANO LETTERS

pubs.acs.org/NanoLett Letter

# High-Performance Organic Photovoltaics Incorporating an Active Layer with a Few Nanometer-Thick Third-Component Layer on a Binary Blend Layer

Hao-Wen Cheng, Chien-Yao Juan, Anisha Mohapatra, Chung-Hao Chen, Yu-Che Lin, Bin Chang, Pei Cheng, Hao-Cheng Wang, Chih Wei Chu, Yang Yang,* and Kung-Hwa Wei*

Cite This: *Nano Lett.* 2021, 21, 2207−2215 Read Online



**ABSTRACT:** In this paper, a universal approach toward constructing a new bilayer device architecture, a few-nanometer-thick third-component layer on a bulk-heterojunction (BHJ) binary blend layer, has been demonstrated in two different state-of-the-art organic photovoltaic (OPV) systems. Through a careful selection of a third component, the power conversion efficiency (PCE) of the device based on PM6/Y6/layered PTQ10 layered third-component structure was 16.8%, being higher than those of corresponding devices incorporating the PM6/Y6/PTQ10 BHJ ternary blend (16.1%) and the PM6/Y6 BHJ binary blend (15.5%). Also, the device featuring PM7/Y1-4F/layered PTQ10 layered third-component structure gave a PCE of 15.2%, which is higher than the PCEs of the devices incorporating the PM7/Y1-4F/PTQ10 BHJ ternary blend and the PM7/Y1-4F BHJ binary blend (14.2 and 14.0%, respectively). These enhancements in PCE based on layered third-component structure can be attributed to improvements in the charge separation and charge collection abilities. This simple concept of the layered third-component structure appears to have great promise for achieving high-performance OPVs.

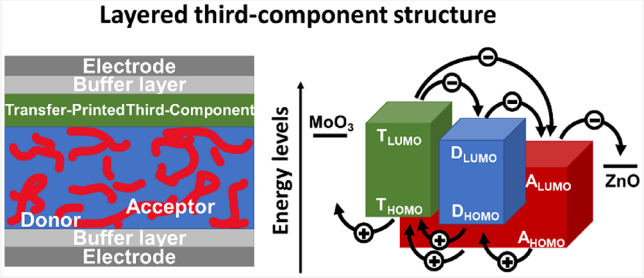


**KEYWORDS:** *organic photovoltaics, layered third component, layered third-component layer structures, bulk heterojunction ternary blend*



Organic photovoltaics (OPVs) are attracting attention as potential renewable energy sources displaying qualities of being flexible, lightweight, and amenable to large-area solution-processing.[1−10] Recent increases in the power conversion efficiencies (PCEs) of OPV devices have resulted from improvements in the design of their nonfullerene acceptors and advances in their devices structures.[11−18] To date, the PCEs of OPV devices have reached over 17%.[19−21]

The evolutionary breakthrough in solution-processed bulk-heterojunction (BHJ) binary blends featuring one donor and one acceptor was first demonstrated in 1995.[22] Because of stronger exciton dissociation ability, such binary-blend devices exhibit PCEs much higher than those of devices based on a single organic semiconductor.[23] Recently, ternary blends have been employed to provide a light absorption spectrum wider than that of binary blends and thereby further enhance the performance of BHJ OPVs.[24−28] One common method for fabricating ternary-blend OPVs has been to mix a third component, either a donor or an acceptor, into a binary blend to form BHJ system.[27,29−32] Compared with BHJ binary-blend systems, devices based on BHJ ternary blends typically show superior performance because of their complementary absorption and modified active layer morphologies.[30,31] Even though much progress has been made in the development of ternary-blend devices, problems associated with the introduction of the third component have limited the extent to which the PCEs have increased. First, an isolated second donor or acceptor domain can retard charge transfer and transport, increasing the likelihood of charge recombination. Second, it has been difficult to control the vertical phase separation in the ternary blend systems. The disordered nature of the BHJ structure makes it possible that undesirable component materials become located at the interface between the active layer and electrode (e.g., acceptor-rich regions located near the anode or donor-rich regions located near the cathode). These drawbacks might hinder the photocurrent that contributes to the efficiency of the device, by limiting the short-circuit current ($J_{sc}$) and the fill factor (FF).[15,33]

A layered third-component bilayer OPV structure, a third-component layer on a BHJ binary-blend layer, might be a viable

**Received:** December 22, 2020
**Revised:** February 9, 2021
**Published:** February 18, 2021

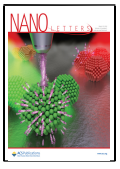




https://dx.doi.org/10.1021/acs.nanolett.0c05045
*Nano Lett.* 2021, 21, 2207−2215

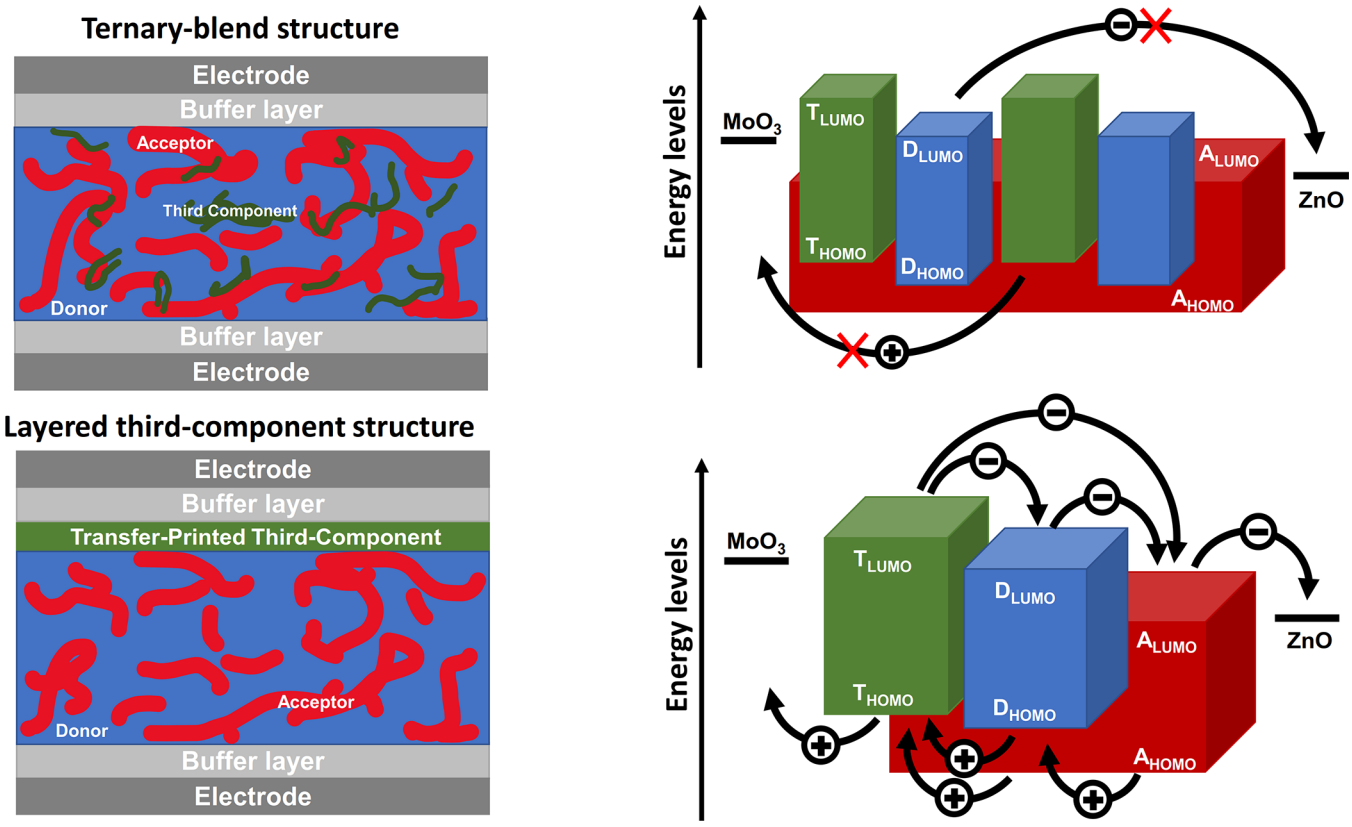


**Figure 1.** Schematic representations of the (a) devices architectures and (b) energy levels of the ternary blend and layered third-component structure [$D_{LUMO}$, lowest unoccupied molecular orbital (LUMO) energy level of the donor; $D_{HOMO}$, highest occupied molecular orbital (HOMO) energy level of the donor; $A_{LUMO}$, LUMO energy level of the acceptor; $A_{HOMO}$, HOMO energy level of the acceptor; $T_{LUMO}$, LUMO energy level of the third component; $T_{HOMO}$, HOMO energy level of the third component].

alternative that overcomes these issues; notably, multilayered structures are used widely in thin film transistors and organic light-emitting diodes.[34−36] A common method toward achieving a multilayer structure, using a cross-linking polymer to render the underlying layer resistant to the top layer, is limited by the choice of available materials and the need to use the orthogonal solvents to prevent damage to the underlying layers.[37−39] Since transfer printing can solve this problem,[40−43] we utilize it in the design of our device structure.

Herein, we describe an approach toward a new layered third-component active layer architecture featuring a layer of the third component on the BHJ binary-blend layer with the requirement that the third component can form cascade lowest unoccupied molecular orbital (LUMO) energy bands relative to the LUMOs of the donor and acceptor of the BHJ binary blend layer. The bilayer structure provides a structure superior to that of the conventional BHJ ternary blend structure. We have prepared layered third-component structures through typical spin-coating of a BHJ binary blend layer and subsequent transfer printing of the third component layer, a polymer donor layer, upon it with transfer printing that does not damage the underlying layer;[42,44,45] we used a stamp of the flexible elastomer polydimethylsiloxane (PDMS) as a scaffold for transferring the donor materials onto the binary blend layer. Compared with devices having the ternary-blend structure (isolated domains), the layered third-component structures appeared to be much more favorable for charge transport to the electrode. To demonstrate the universality of our approach, we prepared systems featuring two different BHJ binary blends (PM6/Y6 and PM7/Y1-4F) and the same third component (PTQ10). The PCEs of the PM6/Y6/layered PTQ10 layered third-component structure devices are up to 16.8% higher than those of devices containing the PM6/Y6/PTQ10 BHJ ternary-blend structure (up to 16.1%) and the PM6/Y6 BHJ binary blend (up to 15.5%). Similarly, the PCEs of the PM7/Y1-4F/layered PTQ10 layered third-component structure devices reached 15.2%, higher than those of the PM7/Y1-4F/PTQ10 BHJ ternary-blend device (14.2%) and the PM7/Y1-4F BHJ binary-blend structure (14.0%). This concept of layered third-component active layers leads to a simple and favorable device architecture for high-performance OPVs.

Figure 1 displays schematic representations of devices having the ternary blend and layered third-component structures. In the ternary-blend structure, the third component is mixed with the donor and acceptor components of the binary blend, leading to formation of isolated domains and inefficient charge transfer between the donor/acceptor components and the third component. In contrast, in the layered third-component structure, the third component is introduced as a pristine layer on top of the BHJ binary-blend layer, eliminating the isolated domains and potentially providing more efficient charge transfer. The band alignment of the materials in this study are provided in the Supporting Information S1.

We chose two benchmark donor/acceptor systems as the binary blends for our active layers: (i) poly[(2,6-(4,8-bis(5-(2-ethylhexyl-3-fluoro)thien-2-yl)-benzo[1,2-*b*:4,5-*b*]-dithiophene))-*alt*-(5,5-(1′,3′-di-2-thienyl-5′,7′-bis(2-ethylhexyl)benzo[1′,2′-*c*:4′,5′-*c*]dithiophene-4,8-dione)]


https://dx.doi.org/10.1021/acs.nanolett.0c05045
Nano Lett. 2021, 21, 2207−2215

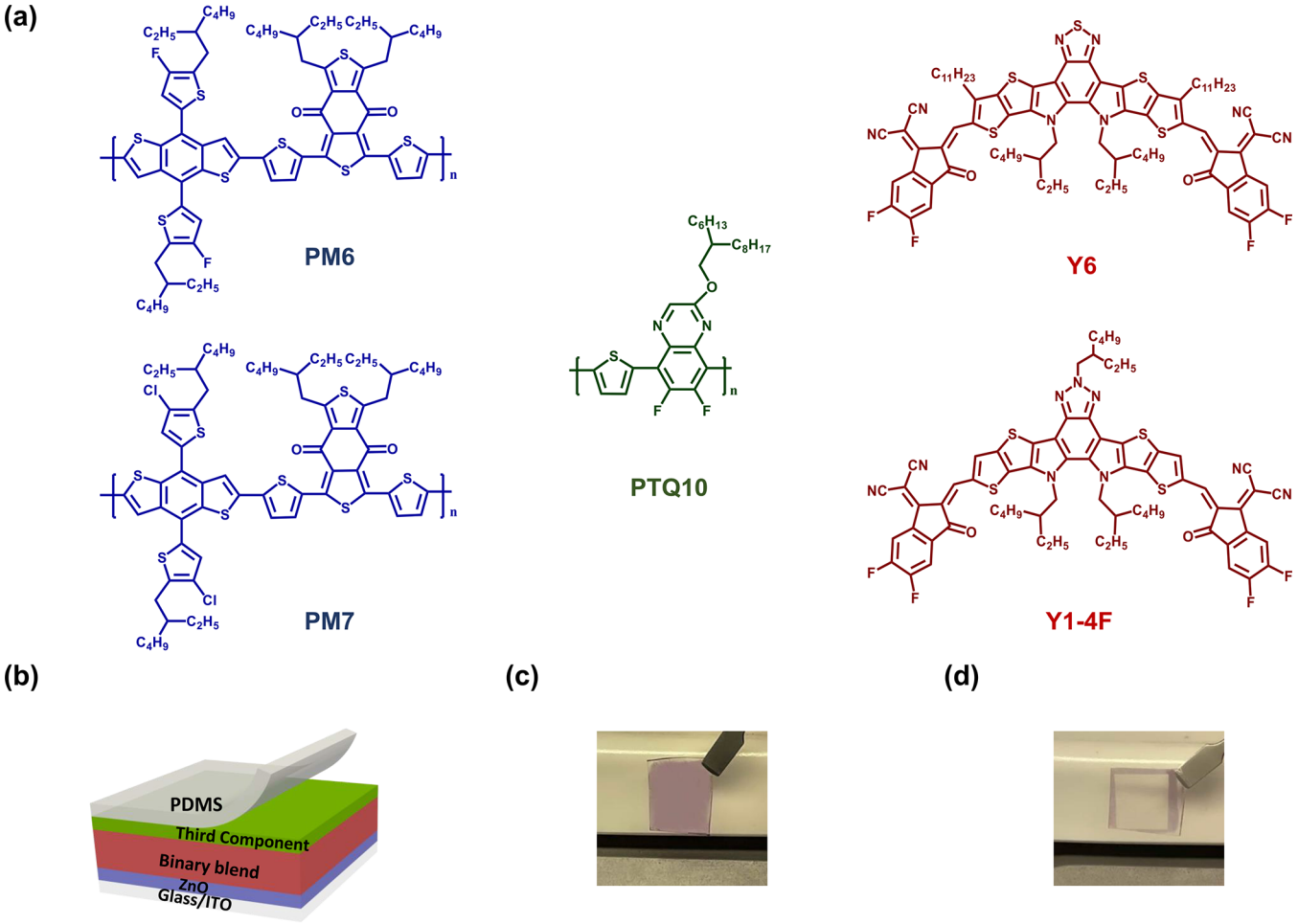


**Figure 2.** (a) Chemical structures of the donors (PM6, PM7) in blue; the acceptors (Y6, Y1-4F) in red; and the third component (PTQ10) in green. (b) Schematic representation (drawn by Quantan Wu and used with permission) of the transfer of the third component onto the binary blend via a PDMS stamp. (c) The photograph of the PTQ10 film on a PDMS stamp. (d) The photograph of the PTQ10 film on a PDMS stamp after being removed.

(PM6)/2,2′-((2*Z*,2′*Z*)-((12,13-bis(2-ethylhexyl)-3,9-diundecyl-12,13-dihydro-[1,2,5]thiadiazolo[3,4-*e*]thieno[2′,3′:4′,5′]thieno[2′,3′:4,5]pyrrolo[3,2-*g*]thieno[2′,3′:4,5]thieno[3,2-*b*]indole-2,10-diyl)bis(methanylylidene))bis(5,6-difluoro-3-oxo-2,3-dihydro-1*H*-indene-2,1-diylidene))dimalononitrile (Y6) and (ii) poly[(2,6-(4,8-bis(5-(2-ethylhexyl-3-chloro)thien-2-yl)-benzo[1,2-*b*:4,5-*b*́]dithiophene))-*alt*-(5,5-(1′,3′-di-2-thienyl-5′,7′-bis(2-ethylhexyl)benzo[1′,2′-*c*:4′,5′-*c*́]dithiophene-4,8-dione)] (PM7)/1-(5-(4,8-bis(5-(2-ethylhexyl)-4-fluorothien-2-yl)-6-methylbenzo[1,2-*b*:4,5-*b*́]dithien-2-yl)thien-2-yl)-5,7-bis(2-ethylhexyl)-3-(5-methylthien-2-yl)-4*H*,8*H*-benzo[1,2-*c*:4,5-*c*́]dithiophene-4,8-dione (Y1-4F). Figure 2a presents the chemical structures of the materials used in this study. The blue structures are the polymer donors (PM6[20] and PM7[46]), the green structure is the third component (PTQ10,[47] poly[(thiophene)-*alt*-(6,7-difluoro-2-(2-hexyldecyloxy)-quinoxaline)]), and the red structures are the small-molecule acceptors (Y6[16] and Y1-4F[48]). We chose PTQ10 as the third component because (i) the LUMO energy level of PTQ10 is higher than that of either PM6 or Y6 in the first case and that of PM7 or Y1-4F in the second case such that the three components form a cascade LUMO energy level and (ii) the PTQ10 has a wider bandgap than that of PM6, PM7, Y6, and Y1-4F, thus providing complementary absorption.

Figure 2b provides a schematic representation of the transfer of the third component using a PDMS stamp. The third component (PTQ10) was first spin-coated onto the stamp; Figure 2c displays a photograph of the PTQ10 film on the PDMS stamp. Next, we attached the PDMS stamp to the BHJ binary blend film and heated the system to 110 °C, causing the PDMS to swell. After 1 min, we peeled off the PDMS stamp, leaving the PTQ10 film behind. Figure 2d shows a photograph of the PDMS stamp after the PTQ10 film was transferred. The transparent rectangular shape is because of the removal of PTQ10 on the PDMS stamp. The thickness of the PTQ10 film is around 10 nm. Details regarding the device fabrication and the method of the estimation the thickness of the PTQ10 film are provided in the Supporting Information.

Figure 3a presents the current density−voltage ($J-V$) characteristics of the devices based on PM6/Y6 (BHJ binary blend), PM6/Y6/PTQ10 (BHJ ternary-blend structure), and PM6/Y6/layered PTQ10 (layered third-component structure) under illumination (100 mW cm$^{-2}$) from an AM 1.5G solar simulator; Table 1 lists the photovoltaic parameters. The layered third-component devices were fabricated having the structure indium tin oxide (ITO)/ZnO/active layer/third component/$MoO_3$/Ag. The average short-circuit current densities ($J_{sc}$) of the devices having the ternary-blend and layered third-component structures (26.5 and 25.8 mA/cm$^2$, respectively)


https://dx.doi.org/10.1021/acs.nanolett.0c05045
Nano Lett. 2021, 21, 2207−2215

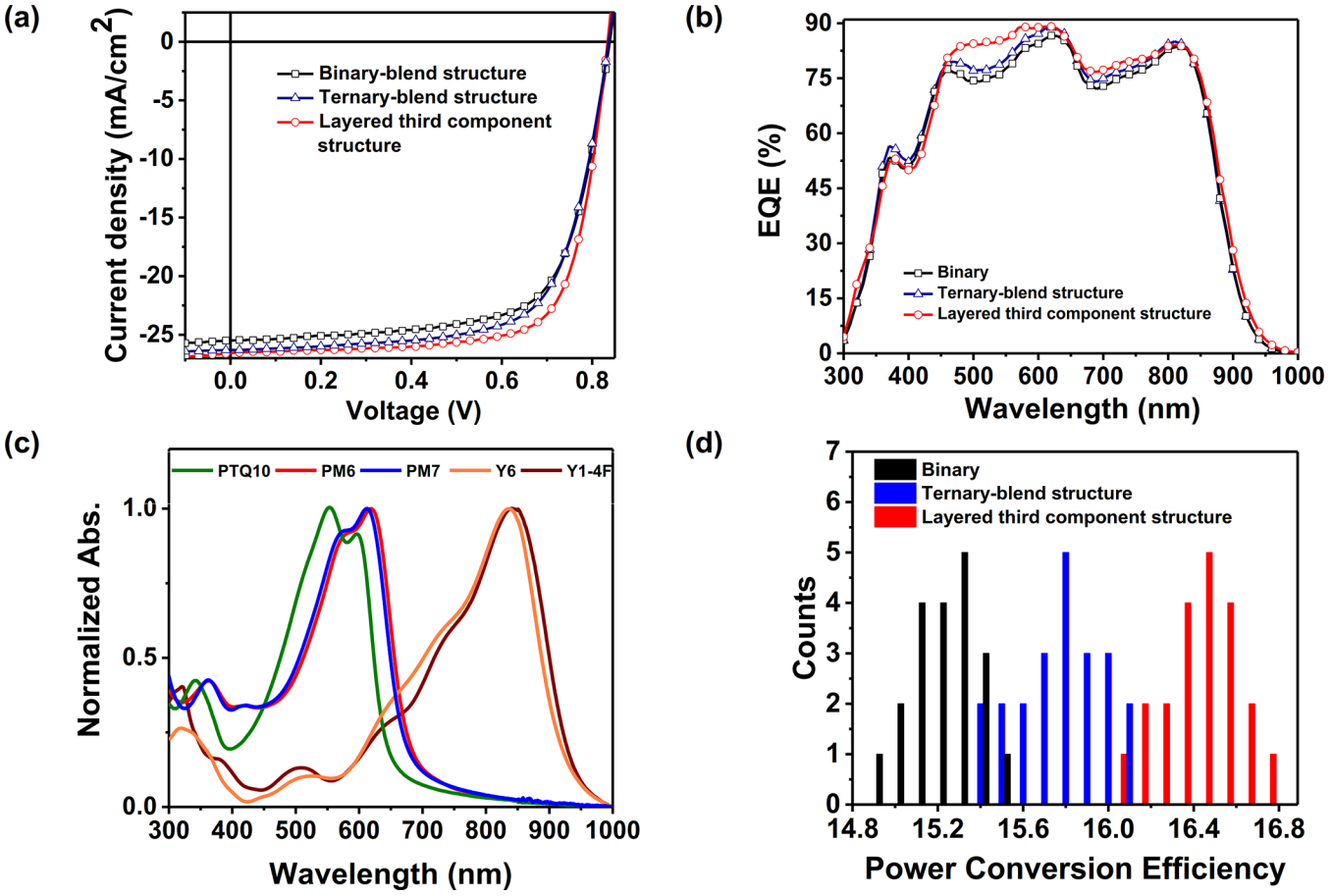


**Figure 3.** (a) $J-V$ curves and (b) EQE spectra of OPV devices based on PM6/Y6 (binary), PM6/Y6/PTQ10 (ternary-blend structure), and PM6/Y6/layered PTQ10 (layered third-component structure). (c) The normalized absorption spectra of pristine PM6, PM7, PTQ10, Y6, and Y1-4F. (d) The distribution of the devices' performance based on PM6/Y6 (binary), PM6/Y6/PTQ10 (ternary-blend structure), and PM6/Y6/PTQ10 (layered third-component structure)

**Table 1. Average and Best Performances of Devices**[a]

| | device structure | $V_{OC}$ (V) | $J_{SC}$ (mA/cm$^2$) | calculated $J_{SC}$ (mA/cm$^2$) | FF (%) | PCE (%) | champion PCE (%) |
|---|---|---|---|---|---|---|---|
| PM6/Y6 | binary | 0.84 ± 0.01 | 25.4 ± 0.2 | 24.9 | 70.2 ± 0.2 | 15.3 ± 0.1 | 15.5 |
| PM6/Y6/PTQ10 | ternary-blend structure | 0.84 ± 0.01 | 25.8 ± 0.5 | 25.6 | 68.0 ± 0.3 | 15.8 ± 0.2 | 16.1 |
| PM6/Y6/ layered PTQ10 | layered third-component structure | 0.84 ±0.01 | 26.5 ± 0.4 | 26.0 | 74.5 ± 0.3 | 16.5 ± 0.2 | 16.8 |
| PTQ10/Y6 | binary | 0.86 ± 0.01 | 24.9 ± 0.2 | 23.5 | 69.3 ± 0.2 | 14.8 ± 0.2 | 15.0 |
| PM7/Y1-4F | binary | 0.83 ± 0.01 | 25.4 ± 0.3 | 23.9 | 65.6 ± 0.1 | 13.8 ± 0.2 | 14.0 |
| PM7/Y1-4F/PTQ10 | ternary-blend structure | 0.84 ± 0.01 | 26.2 ± 0.3 | 24.9 | 63.3 ± 0.2 | 13.9 ± 0.2 | 14.2 |
| PM7/Y1-4F/ layered PTQ10 | layered third-component structure | 0.83 ± 0.01 | 26.1 ± 0.2 | 24.8 | 69.0 ± 0.1 | 14.9 ± 0.2 | 15.2 |
| PTQ10/Y1-4F | binary | 0.85 ± 0.01 | 15.3 ± 0.2 | 14.8 | 52.8 ± 0.1 | 6.8 ± 0.1 | 6.9 |

[a]On the basis of PM6/Y6, PM6/Y6/PTQ10 (ternary-blend structure), PM6/Y6/layered PTQ10 (layered third-component structure), PTQ10/Y6, PM7/Y1-4F, PM7/Y1-4F/PTQ10 (ternary-blend structure), PM7/Y1-4F/layered PTQ10 (layered third-component structure), and PTQ10/Y1-4F.

were greater than that of the binary-blend devices (25.4 mA/cm$^2$). The devices having the layered third-component structure had an average FF (74.5%) higher than those of the devices having the ternary-blend (68.0%) and binary-blend (70.2%) structures. Overall, the devices having the layered third-component structure had a PCE (up to 16.8%) higher than those of the devices having the binary-blend (up to 15.5%) and ternary-blend (up to 16.1%) structures. In comparison, corresponding PTQ10:Y6-based devices exhibited an average PCE of 14.8% with a value of $V_{oc}$ of 0.86 V, a value of $J_{sc}$ of 24.9 mA/cm$^2$, and an FF of 69.3%. Figure 3b displays the external quantum efficiency (EQE) spectra of the devices based on PM6/Y6 (binary blend), PM6/Y6/PTQ10 (ternary-blend structure), and PM6/Y6/layered PTQ10 (layered third-component structure). The measured values of $J_{sc}$ were consistent with those from the integrated EQE spectra. The enhancement in the EQE in the range of 350−650 nm was presumably contributed by the absorption of PTQ10. Figure 3c shows the absorption spectra of the materials in this study. Figure 3d presents the device performance distribution for 20


https://dx.doi.org/10.1021/acs.nanolett.0c05045
Nano Lett. 2021, 21, 2207−2215

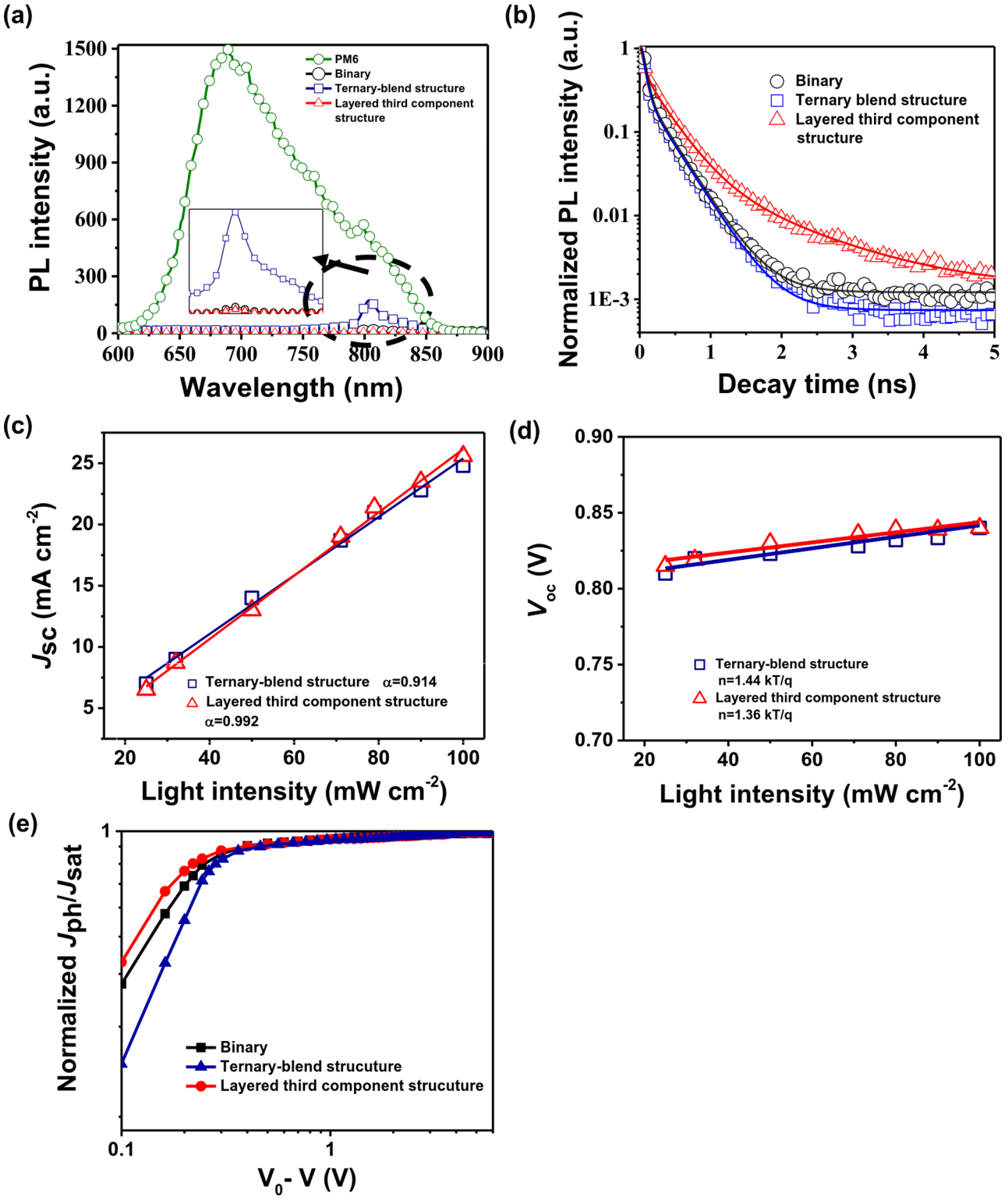


**Figure 4.** (a) PL spectra of pure PM6, PM6/Y6 (binary), PM6/Y6/PTQ10 (ternary-blend structure), and PM6/Y6/layered PTQ10 (layered third-component structure) films; inset: magnified PL spectra. (b) TRPL spectra of PM6/Y6 (binary), PM6/Y6/PTQ10 (ternary-blend structure), and PM6/Y6/layered PTQ10 (layered third-component structure) films. (c,d) The plots of light-dependent photocurrent and photovoltage measurements. (e) Photocurrent data plotted with respect to the effective voltage for devices based on PM6/Y6 (binary), PM6/Y6/PTQ10 (ternary-blend structure), and PM6/Y6/ layered PTQ10 (layered third-component structure).

pieces of devices in total for each condition. To demonstrate the universality of this approach, we also investigated the performance of PM7/Y1-4F-based devices, again fabricated with the device architecture ITO/ZnO/active layer/$MoO_3$/Ag. The average short-circuit current densities ($J_{sc}$) of the PM7/Y1-4F/layered PTQ10 layered third-component structure device were higher than those of the BHJ ternary-blend and binary-blend devices, similar to the trend for the PM6/Y6-based


https://dx.doi.org/10.1021/acs.nanolett.0c05045
Nano Lett. 2021, 21, 2207−2215

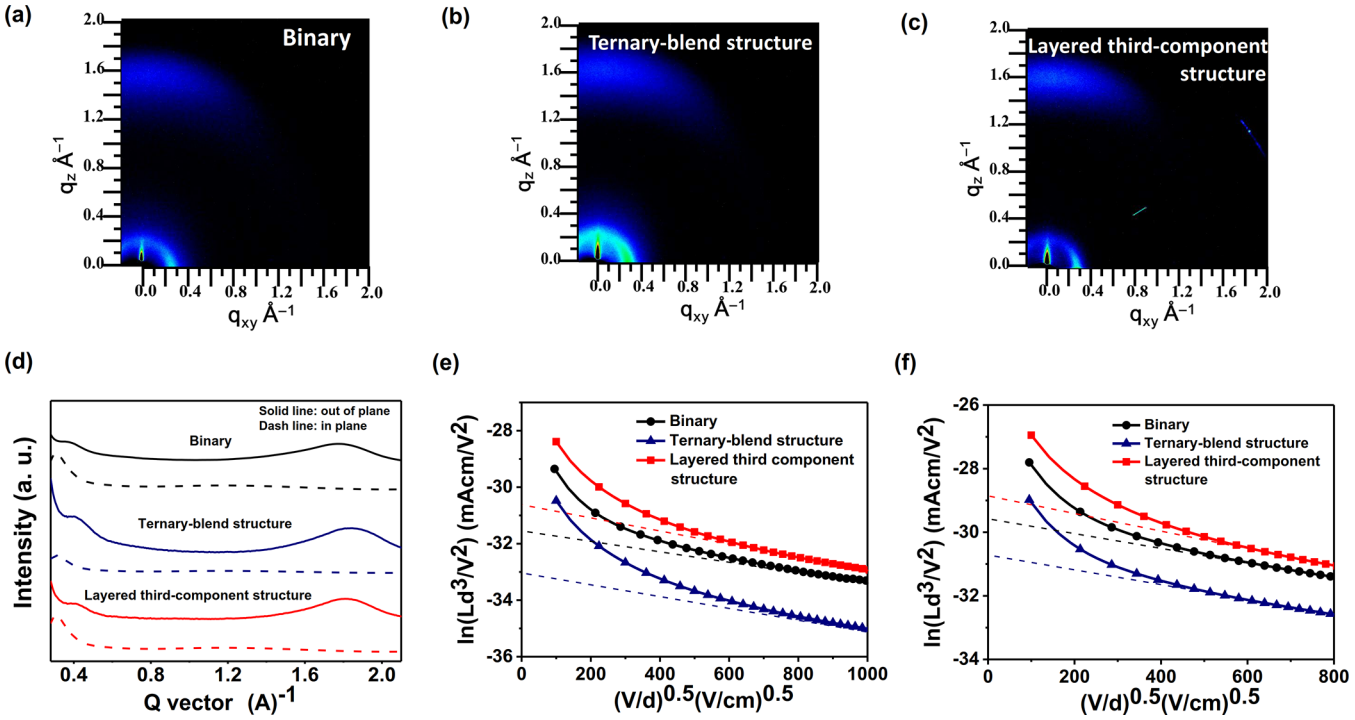


**Figure 5.** (a–c) The 2D GIWAX patterns of films of (a) PM6/Y6 (binary), (b) PM6/Y6/PTQ10 (ternary-blend structure), and (c) PM6/Y6/layered PTQ10 (layered third-component structure). (d) The 1D GIWAX patterns of the films. (d) The one-dimensional GIWAX patterns of each film. (e,f) Hole-only and electron-only device based on PM6/Y6 (binary), PM6/Y6/PTQ10 (ternary-blend structure), and PM6/Y6/layered PTQ10 (layered third-component structure).

devices. Again, we used PTQ10 as the third component. The PM7/Y1-4F/layered PTQ10 (layered third-component structure) devices had an average FF (69.0%) higher than that of the PM7/Y1-4F/PTQ10 (ternary-blend structure) devices (63.3%). Furthermore, the devices having the layered third-component structure had a champion PCE (15.2%) higher than those of the devices based on the binary-blend (14.0%) and ternary-blend (14.2%) structures. For comparison, the PTQ10:Y1-4F-based devices exhibited an average PCE of 6.8% with a $V_{oc}$ of 0.85 V, a $J_{sc}$ of 15.3 mA/cm$^2$, and an FF of 52.8%. The optimized photovoltaic parameters are summarized in Table S1, Table S2, and Table S3. The details of the experimental procedure can be found in the Supporting Information.

We measured photoluminescence (PL) spectra to examine the charge separation ability of each active layer, prepared as a film on a silicon wafer. A higher degree of quenching in the PL spectra indicated stronger charge separation ability. Figure 4a presents the PL spectra of PM6/Y6 (binary), PM6/Y6/PTQ10 (ternary-blend structure), PM6/Y6/layered PTQ10 (layered third-component structure), and pristine PM6 films. Relative to the pristine PM6, the intensities of the PL of the binary-blend, ternary-blend, and layered third-component structures decreased to 99, 92, and 99%, respectively. These values are calculated based on the ratio of the peak area from the active layer films to that of the pristine PM6 film. The relatively low quenching ability of the ternary-blend structure might have resulted from inefficient charge separation between the third component and the donor/acceptor components, caused by reduction of invalid contacts with the third component. We used time-resolved photoluminescence (TRPL) spectroscopy to estimate the exciton lifetimes of the PM6/Y6 (binary), PM6/Y6/PTQ10 (ternary-blend structure), and PM6/Y6/layered PTQ10 (layered third-component structure) films. Figure 4b displays the TRPL decay profile of each film with fitted lines. We calculated the average exciton lifetimes using the equation $\tau_{avg} = A_1\tau_1 + A_2\tau_2$. Among these devices, the one featuring the layered third-component structure displayed the longest average exciton lifetime of 0.208 ns (A1, 0.6294; $\tau$1, 0.0714 ns; A2, 0.4692; $\tau$2, 0.3902 ns). The binary-blend devices provided an average exciton lifetime of 0.152 ns (A1, 1.0347; $\tau$1, 0.1003 ns; A2, 0.1735; $\tau$2, 0.4609 ns). The devices having the ternary-blend structure had the shortest average exciton lifetime of 0.141 ns (A1, 1.0014; $\tau$1, 0.0831 ns; A2, 0.2088; $\tau$2, 0.4201 ns), indicative of a higher possibility of charge recombination, presumably because of poor charge separation ability within its randomly mixed active layer. Table S4 summarizes the fitted parameters of the TRPL spectral decay profiles. In order to understand the charge recombination in the active layer more completely, we carried out measurements of the dependence photocurrent on photovoltage; Figure 4c,d shows the light photocurrent versus photovoltage curves. The relationship between the light intensity ($P$) and the $J_{sc}$ can be described with $J_{sc} \propto P^{\alpha}$. The maximum $\alpha$-value approaches 1 representing the charge transport with negligible bimolecular recombination. The $\alpha$ of layered third-component structure with a value of 0.992 is much closer to unity than that of ternary-blend structure (0.914), indicating the bimolecular recombination is reduced in the layered third-component structure active layer. The relationship of the $V_{oc}$ and $P$ can be expressed as $V_{oc} \propto \frac{nKT}{q} \ln P$ (where $K$ is the Boltzmann constant, $T$ is the absolute temperature, and $q$ is the elementary charge). The slope ($n$) of $V_{oc}$ versus ln($P$) of the ternary-blend structure is 1.44 $\frac{KT}{q}$ which is greater than the value of $\frac{KT}{q}$(0.0259 V), indicating the serious trap-assisted charge


https://dx.doi.org/10.1021/acs.nanolett.0c05045
Nano Lett. 2021, 21, 2207−2215

recombination in ternary-blend structure. However, the slope of the layered third-component structure is a much smaller value ($1.36\ \frac{KT}{q}$), indicating the layered third-component structure could effectively suppress the charge recombination coming from the traps inside the active layer.

To investigate the charge separation and collection abilities of the devices, we measured their corrected photocurrents at various effective voltages. Figure 4 e displays plots of $J_{ph}/J_{sat}$ in the range of the various effective voltages ($V_0 - V$) for the devices incorporating the PM6/Y6 (binary), PM6/Y6/PTQ10 (ternary-blend structure), and PM6/Y6/layered PTQ10 (layered third-component structure) structures. Here, $J_{sat}$ is the saturated current density and $V_{eff}$ is the effective voltage (where $V_{eff} = V_0 - V$; $V$ is the applied voltage; $V_0$ is the voltage when $J_{ph} = 0$). When a large bias was applied to the devices, all of the free charge carriers were collected, leading to a saturated current density ($J_{ph}$). The value of $J_{ph}/J_{sat}$ can be considered as representing the overall charge separation efficiency and charge collection efficiency.[49] When the effective voltage was low, the devices having the ternary-blend structure had lower values of $J_{ph}/J_{sat}$, suggesting poor charge separation and charge collection efficiencies. In comparison, the devices having the layered third-component structure had higher values of $J_{ph}/J_{sat}$ at lower effective voltages, presumably because they avoided isolating the third component. Among our three differently structured devices, those featuring the layered third-component structure had the highest values of $J_{ph}/J_{sat}$ due to their greater charge separation and charge collection abilities. In addition, all of the optimized active layer thicknesses are around 110 nm, and thus the enhancement of the short-circuit current cannot result from the different thickness of the film.

To investigate their molecular packing of the films, we performed two-dimensional (2D) grazing-incidence wide-angle X-ray scattering (GIWAXS).[50] Figures 5a–d presents the one-dimensional (1D) and 2D GIWAXS patterns of the binary-blend film, the ternary-blend structured film, and the layered third-component structured film. The molecular packing in the film of the layered third-component structure was similar to that in the binary-blend film. Compared with the binary-blend film and the layered third-component structure, ternary-blend structure had a slightly stronger intensity (by about 0.3 Å) for $q_z$, presumably because of the nature of the packing of PTQ10; Figure S2 (Supporting Information) presents the GIWAXS pattern of PTQ10. For the film having the ternary-blend structure, the incorporation of PTQ10 (third component) changed the molecular packing in the active layer. The introduction of the third component might have created an invalid charge-transfer interface, resulting in a lower FF for the devices having the ternary-blend structure. We adopted the space charge limited current (SCLC) method to measure the electron and hole mobilities. We prepared electron-only and hole-only devices having the structure ITO/PEDOT:PSS/active layer/$MoO_3$/Ag and ITO/Al/active layer/Al, respectively. Figure 5e,f represents the dark $J-V$ curves for the devices incorporating the PM6/Y6 (binary), PM6/Y6/PTQ10 (ternary-blend structure), and PM6/Y6/layered PTQ10 (layered third-component structure) structures. The devices having the layered third-component structure displayed electron and hole mobilities ($3.0 \times 10^{-4}$ cm$^2$ V$^{-1}$ s$^{-1}$ for electron-only; $1.7 \times 10^{-3}$ cm$^2$ V$^{-1}$ s$^{-1}$ for hole-only) higher than those of the binary-blend devices ($1.1 \times 10^{-4}$ cm$^2$ V$^{-1}$ s$^{-1}$ for electron-only; $9.1 \times 10^{-4}$ cm$^2$ V$^{-1}$ s$^{-1}$ for hole-only). In comparison, the devices having the ternary-blend structure had poor electron and hole mobilities ($1.5 \times 10^{-5}$ cm$^2$ V$^{-1}$ s$^{-1}$ for electron-only; $2.7 \times 10^{-4}$ cm$^2$ V$^{-1}$ s$^{-1}$ for hole-only), presumably because the random mixing of the third component into the active layer led to inefficient charge transfer between the third component and the donor/acceptor components. Table S5 summarizes the mobility data. In addition, the stability of the OPVs with different active layer structures, PM6/Y6 (binary), PM6/Y6/PTQ10 (ternary-blend), and PM6/Y6/PTQ10 (layered third-component), have been tested at 130 °C. Figure S3 shows the stability curves of the PCEs of the devices with three different active layer structures at different heating times. The binary and the ternary-blend-based devices show their PCEs having relatively steep drops in the first 10 min, as compared to the case of the layered third-component-based device. After 20 min of annealing, the value of the PCE of the layered third-component-based device still maintains around 90% of its original PCE value; the PCEs of the binary and the ternary-blend-based devices, however, remain less than 80% of their original PCE. After 60 min of annealing, the value of the PCE of the layered third-component device remains 75% of the original PCE value; the binary and the ternary-blend-based devices, however, remain less than 70% of their original PCE. Overall, the layered third-component-based device shows the best stability at 130 °C for a period of 60 min among the three different kinds of active layer structure.

In summary, we have used transfer printing to prepare novel active layer architectures (layered third-component structures) for binary-blend BHJs and a third-component polymer donor. Overall, the devices with having the layered third-component structure had much more efficient charge separation and charge collection abilities than those of the corresponding devices having ternary-blend and binary-blend structures. The best PCEs for the devices incorporating PM6/Y6/layered PTQ10 and PM7/Y1-4F/layered PTQ10 (i.e., layered third-component structures) were 16.8 and 15.2%, respectively; these values are higher than those of the corresponding ternary-blend devices (16.1 and 14.2%, respectively) and binary-blend devices (15.5 and 14.0%, respectively). These PCEs and stabilities reveal the superiority of the devices having the layered third-component structures, prepared using transfer-printing, over traditional ternary-blend devices. We anticipate that this facile fabrication procedure will lead to OPVs pursuing even higher performance.

## ■ ASSOCIATED CONTENT

### Supporting Information

The Supporting Information is available free of charge at https://pubs.acs.org/doi/10.1021/acs.nanolett.0c05045.

Band alignment, GIWAX pattern, photovoltaic performance tables (PDF)

## ■ AUTHOR INFORMATION

### Corresponding Authors

**Kung-Hwa Wei** − *Department of Materials Science and Engineering, Center for Emergent Functional Matter Science, National Chiao Tung University, Hsinchu 3001, Taiwan; Department of Materials Science and Engineering, National Yang Ming Chiao Tung University, Hsinchu 3001, Taiwan;* orcid.org/0000-0002-0248-4091; Email: khwei@mail.nctu.edu.tw

**Yang Yang** − *Department of Materials Science and Engineering, California NanoSystems Institute, University of California, Los*



https://dx.doi.org/10.1021/acs.nanolett.0c05045
Nano Lett. 2021, 21, 2207−2215

*Angeles, California 90095, United States;* orcid.org/0000-0001-8833-7641; Email: yangy@ucla.edu

### Authors

**Hao-Wen Cheng** – *Department of Materials Science and Engineering, Center for Emergent Functional Matter Science, National Chiao Tung University, Hsinchu 3001, Taiwan; Department of Materials Science and Engineering, National Yang Ming Chiao Tung University, Hsinchu 3001, Taiwan;* orcid.org/0000-0003-1940-7962

**Chien-Yao Juan** – *Department of Materials Science and Engineering, Center for Emergent Functional Matter Science, National Chiao Tung University, Hsinchu 3001, Taiwan; Department of Materials Science and Engineering, National Yang Ming Chiao Tung University, Hsinchu 3001, Taiwan*

**Anisha Mohapatra** – *Research Center for Applied Science, Academia Sinica, Taipei 115, Taiwan*

**Chung-Hao Chen** – *Department of Materials Science and Engineering, Center for Emergent Functional Matter Science, National Chiao Tung University, Hsinchu 3001, Taiwan; Department of Materials Science and Engineering, National Yang Ming Chiao Tung University, Hsinchu 3001, Taiwan*

**Yu-Che Lin** – *Department of Materials Science and Engineering, Center for Emergent Functional Matter Science, National Chiao Tung University, Hsinchu 3001, Taiwan; Department of Materials Science and Engineering, National Yang Ming Chiao Tung University, Hsinchu 3001, Taiwan*

**Bin Chang** – *Department of Materials Science and Engineering, Center for Emergent Functional Matter Science, National Chiao Tung University, Hsinchu 3001, Taiwan; Department of Materials Science and Engineering, National Yang Ming Chiao Tung University, Hsinchu 3001, Taiwan*

**Pei Cheng** – *Department of Materials Science and Engineering, California NanoSystems Institute, University of California, Los Angeles, California 90095, United States;* orcid.org/0000-0002-1012-749X

**Hao-Cheng Wang** – *Department of Materials Science and Engineering, Center for Emergent Functional Matter Science, National Chiao Tung University, Hsinchu 3001, Taiwan; Department of Materials Science and Engineering, National Yang Ming Chiao Tung University, Hsinchu 3001, Taiwan*

**Chih Wei Chu** – *Research Center for Applied Science, Academia Sinica, Taipei 115, Taiwan;* orcid.org/0000-0003-0979-1729

Complete contact information is available at: https://pubs.acs.org/10.1021/acs.nanolett.0c05045

### Author Contributions

The manuscript was written with contributions from all of the authors, who have given approval to the final version of the manuscript.

### Notes

The authors declare no competing financial interest.

## ■ ACKNOWLEDGMENTS

K.-H.W. thanks the Center for Emergent Functional Matter Science of National Yang Ming Chiao Tung University/National Chiao Tung University from the Featured Areas Research Center Program within the framework of the Higher Education Sprout Project by the Ministry of Education (MOE), Taiwan; the Ministry of Science and Technology, Taiwan (MOST 109-2221-E-009-064-MY3, MOST 107-2923-M-009-004-MY3); and the Ministry of Education Subsidies for Universities and Tertiary Colleges to Develop International Bilateral Program to Jointly Train World Class Professionals, Taiwan, for financial support. Y.Y. thanks the Air Force Office of Scientific Research (AFOSR, FA2386-18-1-4094) for financial support. We thank Dr. Quantan Wu for drawing Figure 2b.

## ■ REFERENCES

(1) Graetzel, M.; Janssen, R. A. J.; Mitzi, D. B.; Sargent, E. H. Materials Interface Engineering for Solution-Processed Photovoltaics. *Nature* **2012**, *488* (7411), 304–312.

(2) Janssen, R. A. J.; Nelson, J. Factors Limiting Device Efficiency in Organic Photovoltaics. *Adv. Mater.* **2013**, *25* (13), 1847–1858.

(3) Huang, Y.; Kramer, E. J.; Heeger, A. J.; Bazan, G. C. Bulk Heterojunction Solar Cells: Morphology and Performance Relationships. *Chem. Rev.* **2014**, *114* (14), 7006–7043.

(4) Fan, Q.; Wang, Y.; Zhang, M.; Wu, B.; Guo, X.; Jiang, Y.; Li, W.; Guo, B.; Ye, C.; Su, W.; Fang, J.; Ou, X.; Liu, F.; Wei, Z.; Sum, T. C.; Russell, T. P.; Li, Y. High-Performance As-Cast Nonfullerene Polymer Solar Cells with Thicker Active Layer and Large Area Exceeding 11% Power Conversion Efficiency. *Adv. Mater.* **2018**, *30* (6), 1704546.

(5) Zhang, G.; Zhao, J.; Chow, P. C. Y.; Jiang, K.; Zhang, J.; Zhu, Z.; Zhang, J.; Huang, F.; Yan, H. Nonfullerene Acceptor Molecules for Bulk Heterojunction Organic Solar Cells. *Chem. Rev.* **2018**, *118* (7), 3447–3507.

(6) Hou, J.; Inganäs, O.; Friend, R. H.; Gao, F. Organic Solar Cells Based on Non-Fullerene Acceptors. *Nat. Mater.* **2018**, *17* (2), 119–128.

(7) Yan, C.; Barlow, S.; Wang, Z.; Yan, H.; Jen, A. K. Y.; Marder, S. R.; Zhan, X. Non-Fullerene Acceptors for Organic Solar Cells. *Nature Reviews Materials.* **2018**, *3*, 18003.

(8) Cheng, P.; Li, G.; Zhan, X.; Yang, Y. Next-Generation Organic Photovoltaics Based on Non-Fullerene Acceptors. *Nat. Photonics* **2018**, *12* (3), 131–142.

(9) Li, W.; Yao, H.; Zhang, H.; Li, S.; Hou, J. Potential of Nonfullerene Small Molecules with High Photovoltaic Performance. *Chem. - Asian J.* **2017**, *12* (17), 2160–2171.

(10) Su, Y. W.; Lan, S. C.; Wei, K. H. Organic Photovoltaics. *Mater. Today* **2012**, *15* (12), 554–562.

(11) Li, Y. Molecular Design of Photovoltaic Materials for Polymer Solar Cells: Toward Suitable Electronic Energy Levels and Broad Absorption. *Acc. Chem. Res.* **2012**, *45* (5), 723–733.

(12) Lin, Y.; Wang, J.; Zhang, Z.-G.; Bai, H.; Li, Y.; Zhu, D.; Zhan, X. An Electron Acceptor Challenging Fullerenes for Efficient Polymer Solar Cells. *Adv. Mater.* **2015**, *27* (7), 1170–1174.

(13) Yuan, J.; Huang, T.; Cheng, P.; Zou, Y.; Zhang, H.; Yang, J.; Chang, S.-Y.; Zhang, Z.; Huang, W.; Wang, R.; Meng, D.; Gao, F.; Yang, Y. Enabling Low Voltage Losses and High Photocurrent in Fullerene-Free Organic Photovoltaics. *Nat. Commun.* **2019**, *10* (1), 1–8.

(14) Kumar, A.; Li, G.; Hong, Z.; Yang, Y. High Efficiency Polymer Solar Cells with Vertically Modulated Nanoscale Morphology. *Nanotechnology* **2009**, *20* (16), 165202 DOI: 10.1088/0957-4484/20/16/165202.

(15) Cheng, P.; Wang, R.; Zhu, J.; Huang, W.; Chang, S.-Y.; Meng, L.; Sun, P.; Cheng, H.-W.; Qin, M.; Zhu, C.; et al. Ternary System with Controlled Structure: A New Strategy toward Efficient Organic Photovoltaics. *Adv. Mater.* **2018**, *30* (8), 1705243.

(16) Yuan, J.; Zhang, Y.; Zhou, L.; Zhang, G.; Yip, H.-L.; Lau, T.-K.; Lu, X.; Zhu, C.; Peng, H.; Johnson, P. A.; et al. Single-Junction Organic Solar Cell with over 15% Efficiency Using Fused-Ring Acceptor with Electron-Deficient Core. *Joule* **2019**, *3* (4), 1140–1151.

(17) Lin, Y.; He, Q.; Zhao, F.; Huo, L.; Mai, J.; Lu, X.; Su, C. J.; Li, T.; Wang, J.; Zhu, J.; et al. A Facile Planar Fused-Ring Electron Acceptor for As-Cast Polymer Solar Cells with 8.71% Efficiency. *J. Am. Chem. Soc.* **2016**, *138* (9), 2973–2976.

(18) Wang, H. C.; Cheng, P.; Tan, S.; Chen, C. H.; Chang, B.; Tsao, C. S.; Chen, L. Y.; Hsieh, C. A.; Lin, Y. C.; Cheng, H. W. Sequential Deposition of Donor and Acceptor Provides High-Performance

Semitransparent Organic Photovoltaics Having a Pseudo p-i-n Active Layer Structure. *Adv. Energy Mater.* **2021**, 2003576.
(19) Cui, Y.; Yao, H.; Zhang, J.; Xian, K.; Zhang, T.; Hong, L.; Wang, Y.; Xu, Y.; Ma, K.; An, C.; He, C.; Wei, Z.; Gao, F.; Hou, J.; et al. Single-Junction Organic Photovoltaic Cells with Approaching 18% Efficiency. *Adv. Mater.* **2020**, *32*, 1908205.
(20) Zhan, L.; Li, S.; Lau, T.-K.; Cui, Y.; Lu, X.; Shi, M.; Li, C.-Z.; Li, H.; Hou, J.; Chen, H. Over 17% Efficiency Ternary Organic Solar Cells Enabled by Two Non-Fullerene Acceptors Working in an Alloy-like Model. *Energy Environ. Sci.* **2020**, *13*, 635−645.
(21) Meng, L.; Zhang, Y.; Wan, X.; Li, C.; Zhang, X.; Wang, Y.; Ke, X.; Xiao, Z.; Ding, L.; Xia, R.; Yip, H.-L.; Cao, Y.; Chen, Y.; et al. Organic and Solution-Processed Tandem Solar Cells with 17.3% Efficiency. *Science (Washington, DC, U. S.)* **2018**, *361*, 1094.
(22) Yu, G.; Gao, J.; Hummelen, J. C.; Wudl, F.; Heeger, A. J. Polymer Photovoltaic Cells: Enhanced Efficiencies via a Network of Internal Donor-Acceptor Heterojunctions. *Science (Washington, DC, U. S.)* **1995**, *270* (5243), 1789−1791.
(23) Tang, C. W. Two-Layer Organic Photovoltaic Cell. *Appl. Phys. Lett.* **1986**, *48* (2), 183−185.
(24) Lu, L.; Chen, W.; Xu, T.; Yu, L. High-Performance Ternary Blend Polymer Solar Cells Involving Both Energy Transfer and Hole Relay Processes. *Nat. Commun.* **2015**, *6*, 7327.
(25) Cheng, H.-W.; Zhang, H.; Lin, Y.; She, N.; Wang, R.; Chen, C.; Yuan, J.; Tsao, C.; Yabushita, A.; Zou, Y.; et al. Realizing Efficient Charge/Energy Transfer and Charge Extraction in Fullerene-Free Organic Photovoltaics via a Versatile Third Component. *Nano Lett.* **2019**, *19* (8), 5053−5061.
(26) Cheng, P.; Wang, J.; Zhang, Q.; Huang, W.; Zhu, J.; Wang, R.; Chang, S.; Sun, P.; Meng, L.; Zhao, H.; et al. Unique Energy Alignments of a Ternary Material System toward High-Performance Organic Photovoltaics. *Adv. Mater.* **2018**, *30* (28), 1801501.
(27) Lu, L.; Xu, T.; Chen, W.; Landry, E. S.; Yu, L. Ternary Blend Polymer Solar Cells with Enhanced Power Conversion Efficiency. *Nat. Photonics* **2014**, *8* (9), 716−722.
(28) Lin, Y.-C.; Cheng, H.-W.; Su, Y.-W.; Lin, B.-H.; Lu, Y.-J.; Chen, C.-H.; Chen, H.-C.; Yang, Y.; Wei, K. H. Molecular Engineering of Side Chain Architecture of Conjugated Polymers Enhances Performance of Photovoltaics by Tuning Ternary Blend Structures. *Nano Energy* **2018**, *43*, 138−148.
(29) Huang, W.; Cheng, P.; Yang, Y. M.; Li, G.; Yang, Y. High-Performance Organic Bulk-Heterojunction Solar Cells Based on Multiple-Donor or Multiple-Acceptor Components. *Adv. Mater.* **2018**, *30* (8), 1705706.
(30) Zhang, J.; Zhang, Y.; Fang, J.; Lu, K.; Wang, Z.; Ma, W.; Wei, Z. Conjugated Polymer-Small Molecule Alloy Leads to High Efficient Ternary Organic Solar Cells. *J. Am. Chem. Soc.* **2015**, *137* (25), 8176−8183.
(31) Baran, D.; Ashraf, R. S.; Hanifi, D. A.; Abdelsamie, M.; Gasparini, N.; Röhr, J. A.; Holliday, S.; Wadsworth, A.; Lockett, S.; Neophytou, M.; et al. Reducing the Efficiency-Stability-Cost Gap of Organic Photovoltaics with Highly Efficient and Stable Small Molecule Acceptor Ternary Solar Cells. *Nat. Mater.* **2017**, *16* (3), 363−369.
(32) Chang, B.; Cheng, H. W.; Lin, Y. C.; Wang, H. C.; Chen, C. H.; Nguyen, V. T.; Yang, Y.; Wei, K. H. Incorporating Indium Selenide Nanosheets into a Polymer/Small Molecule Binary Blend Active Layer Enhances the Long-Term Stability and Performance of Its Organic Photovoltaics. *ACS Appl. Mater. Interfaces* **2020**, *12* (49), 55023−55032.
(33) Cheng, H. W.; Raghunath, P.; Wang, K. L.; Cheng, P.; Haung, T.; Wu, Q.; Yuan, J.; Lin, Y. C.; Wang, H. C.; Zou, Y.; et al. Potassium-Presenting Zinc Oxide Surfaces Induce Vertical Phase Separation in Fullerene-Free Organic Photovoltaics. *Nano Lett.* **2020**, *20* (1), 715−721.
(34) Chabinyc, M. L.; Salleo, A.; Wu, Y.; Liu, P.; Ong, B. S.; Heeney, M.; McCulloch, I. Lamination Method for the Study of Interfaces in Polymeric Thin Film Transistors. *J. Am. Chem. Soc.* **2004**, *126* (43), 13928−13929.
(35) Guo, T. F.; Pyo, S.; Chang, S. C.; Yang, Y. High Performance Polymer Light-Emitting Diodes Fabricated by a Low Temperature Lamination Process. *Adv. Funct. Mater.* **2001**, *11* (5), 339−343.
(36) Gong, X.; Wang, S.; Moses, D.; Bazan, G. C.; Heeger, A. J. Multilayer Polymer Light-Emitting Diodes: White-Light Emission with High Efficiency. *Adv. Mater.* **2005**, *17* (17), 2053−2058.
(37) Rumer, J. W.; McCulloch, I. Organic Photovoltaics: Crosslinking for Optimal Morphology and Stability. *Mater. Today* **2015**, *18* (8), 425−435.
(38) Cheng, Y. J.; Hsieh, C. H.; Li, P. J.; Hsu, C. S. Morphological Stabilization by in Situ Polymerization of Fullerene Derivatives Leading to Efficient, Thermally Stable Organic Photovoltaics. *Adv. Funct. Mater.* **2011**, *21* (9), 1723−1732.
(39) Van Franeker, J. J.; Kouijzer, S.; Lou, X.; Turbiez, M.; Wienk, M. M.; Janssen, R. A. J. Depositing Fullerenes in Swollen Polymer Layers via Sequential Processing of Organic Solar Cells. *Adv. Energy Mater.* **2015**, *5* (14), 1500464.
(40) Yim, K. H.; Zheng, Z.; Liang, Z.; Friend, R. H.; Huck, W. T. S.; Kim, J. S. Efficient Conjugated-Polymer Optoelectronic Devices Fabricated by Thin-Film Transfer-Printing Technique. *Adv. Funct. Mater.* **2008**, *18* (7), 1012−1019.
(41) Mohapatra, A.; Singh, A.; Abbas, S. A.; Lu, Y. J.; Boopathi, K. M.; Hanmandlu, C.; Kaisar, N.; Lee, C. H.; Chu, C. W. Bilayer Polymer Solar Cells Prepared with Transfer Printing of Active Layers from Controlled Swelling/de-Swelling of PDMS. *Nano Energy* **2019**, *63* (June), 103826.
(42) Hoth, C. N.; Schilinsky, P.; Choulis, S. A.; Brabec, C. J. Printing Highly Efficient Organic Solar Cells. *Nano Lett.* **2008**, *8* (9), 2806−2813.
(43) Huang, J. H.; Ho, Z. Y.; Kuo, T. H.; Kekuda, D.; Chu, C. W.; Ho, K. C. Fabrication of Multilayer Organic Solar Cells through a Stamping Technique. *J. Mater. Chem.* **2009**, *19* (24), 4077−4080.
(44) Yoon, J.; Baca, A. J.; Park, S. Il; Elvikis, P.; Geddes, J. B.; Li, L.; Kim, R. H.; Xiao, J.; Wang, S.; Kim, T. H.; et al. Ultrathin Silicon Solar Microcells for Semitransparent, Mechanically Flexible and Micro-concentrator Module Designs. *Nat. Mater.* **2008**, *7* (11), 907−915.
(45) Wang, C.; Linghu, C.; Nie, S.; Li, C.; Lei, Q.; Tao, X.; Zeng, Y.; Du, Y.; Zhang, S.; Yu, K.; Jin, H.; Chen, W.; Song, J.; et al. Programmable and Scalable Transfer Printing with High Reliability and Efficiency for Flexible Inorganic Electronics. *Sci. Adv.* **2020**, *6* (25), eabb2393.
(46) Zhang, S.; Qin, Y.; Zhu, J.; Hou, J. Over 14% Efficiency in Polymer Solar Cells Enabled by a Chlorinated Polymer Donor. *Adv. Mater.* **2018**, *30* (20), 1800868.
(47) Sun, C.; Pan, F.; Bin, H.; Zhang, J.; Xue, L.; Qiu, B.; Wei, Z.; Zhang, Z. G.; Li, Y. A Low Cost and High Performance Polymer Donor Material for Polymer Solar Cells. *Nat. Commun.* **2018**, *9* (1), 1−10.
(48) Wang, R.; Yuan, J.; Wang, R.; Han, G.; Huang, T.; Huang, W.; Xue, J.; Wang, H.; Zhang, C.; Zhu, C.; et al. Rational Tuning of Molecular Interaction and Energy Level Alignment Enables High-Performance Organic Photovoltaics. *Adv. Mater.* **2019**, *31* (43), 1904215.
(49) Faist, M. A.; Shoaee, S.; Tuladhar, S.; Dibb, G. F. A.; Foster, S.; Gong, W.; Kirchartz, T.; Bradley, D. D. C.; Durrant, J. R.; Nelson, J. Understanding the Reduced Efficiencies of Organic Solar Cells Employing Fullerene Multiadducts as Acceptors. *Adv. Energy Mater.* **2013**, *3* (6), 744−752.
(50) Chiu, M. Y.; Jeng, U. S.; Su, C. H.; Liang, K. S.; Wei, K. H. Simultaneous Use of Small- and Wide-Angle X-Ray Techniques to Analyze Nanometerscale Phase Separation in Polymer Heterojunction Solar Cells. *Adv. Mater.* **2008**, *20* (13), 2573−2578.


https://dx.doi.org/10.1021/acs.nanolett.0c05045
*Nano Lett.* 2021, 21, 2207−2215